Journal of Innovative Technology, Vol. 4, No. 1, pp. 45-55, March 2022
http://doi.org/10.29424/JIT.202203_4(1).0008

Resonant Converter with Bi-directional Power Flow and Balance Currents

Bor-Ren Lin [1*] and Yen-Chieh Huang [2]

ABSTRACT

This research paper concerns the implementation of a direct current to direct current zero voltage operation converter with an addition parallel inductor and a current balance magnetic so as to realize high circuit efficiency, balance secondary-side currents and achieve bi-directional power flow. The studied resonant converter was determined by a frequency-control half-bridge circuit on the primary side and two parallel full-wave rectifier circuits on the secondary side. Series resonant tank was employed on primary side to achieve the advantage of low switching losses of power devices on primary and secondary sides. The current balance issue of two center-tapped rectifiers on low voltage side was realized by a current balance magnetic-coupling core. Power switches were used on both of the primary and secondary sides to reduce the conduction losses and achieve bi-directional power flow capability. The performance of the presented circuit was confirmed by a laboratory prototype with 720W rated power.

Keywords: Resonant converter, Soft switching, Bi-directional power flow.

1. INTRODUCTION

To better lessen global greenhouse effect and air pollution, great progress has been made in power electronics base renewable energy sources over the past several years. Bi-directional converters (Ahrabi *et al*. 2017; Emadi *et al*. 2008; Lee *et al*. 2012; Mangu *et al*. 2016; Mishimay *et al*. 2010; Shen *et al*. 2017; Yilmaz and Krein 2013; Zhang, Gao, and Li 2018) have been proposed for battery chargers, energy storage systems, dc micro-grid systems and electric vehicles to achieve bi-directional power flow capability. As far as dc micro-grid systems are concerned, bi-directional dc-dc converters can better save energy into energy storage systems in normal conditions and so release power to dc bus when there is a power shortage of dc utility power. Moreover, when it comes to electric vehicles (Ahrabi *et al*. 2017; Emadi *et al*. 2008; Yilmaz and Krein 2013), power converters are generally employed for battery charger, motor drive and dc power distribution. Likewise, as to conventional bi-directional power flow, symmetric circuit topologies with full bridge circuit and half bridge circuit have been developed in dc micro-grid systems and electric vehicles applications. Dual active bridge topologies (Wu *et al*. 2015; Xu *et al*. 2018) with phase-shift modulation between two active bridges and the LLC topologies (Jiang *et al*. 2015; Kim *et al*. 2014; Tan *et al*. 2014) have been also studied to satisfy advantages of zero voltage switching operation and symmetric circuit topology. The main disadvantages of dual active bridge converter are that this device can exhibit high conduction loss. This mainly due to high circulating current, and so it is hard to be implemented by analog integrated circuit. The symmetric resonant circuit topologies with full bridge circuit have been employed (Jiang *et al*. 2015; Kim *et al*. 2014; Tan *et al*. 2014) to overcome the drawback of dual active bridges so that power switches can better realize soft switching operation and lessen electromagnetic interference. But a parallel inductor is attached onto the half bridge leg. In this case, it tends to increase conduction loss and reduce circuit efficiency at forward power flow operation. Likewise, the CLLC bi-directional converters (Zhang *et al*. 2018; Zhao *et al*. 2018; Zou *et al*. 2018) can achieve bidirectional power transfer due to symmetric circuit topologies on the primary and secondary sides for utility power flow control and electric vehicle battery charger systems. However, the CLLC converters are operated well for medium voltage applications. The main disadvantage of the CLLC converters on low voltage applications is the high current stress of resonant capacitor on low voltage side.

In this research, a new soft switching frequency-control converter was studied to realize (1) bi-directional power operation, (2) zero voltage operation for active switches, (3) current sharing on high current side, and (4) high circuit efficiency. Regarding the presented converter, the half bridge leg is used on the primary (high voltage) side, and two parallel center-tapped rectifiers are employed on the secondary (high current) side. The load voltage control is tested through variable frequency scheme to adjust the voltage gain of the proposed circuit. An additional inductor is adopted on the primary side under reverse power operation to realize bidirectional power flow. Since the LLC circuit tank is used on the primary side for both power flow operations, the power devices are all turned on at zero voltage switching to achieve high circuit efficiency instead. Besides, to realize current sharing function, a magnetic-coupling current balance component is employed on the high current side. The effectiveness of the presented circuit is verified and confirmed by the experimental results.

Manuscript received July 1, 2021; accepted July 22, 2021.

[1*] Professor (corresponding author), Department of Electrical Engineering, National Yunlin University of Science and Technology, Yunlin, Taiwan 64002, R.O.C. (e-mail: linbr@yuntech.edu.tw).

[2] Graduate Student, Department of Electrical Engineering, National Yunlin University of Science and Technology, Yunlin, Taiwan 64002, R.O.C.

2. CIRCUIT DIAGRAM, OPERATION PRINCIPLE AND CIRCUIT CHARACTERISTICS

The basic structure of series resonant converter is a half bridge leg on high voltage side and a full-wave rectifier with fast recovery

diodes on low voltage side to realize low switching losses and low reverse recovery current losses. The synchronous switches can be adopted on the secondary-side to decrease conduction losses as depicted in Fig. 1(a). However, the circuit structure, as can be seen from Fig. 1(a), is not easier to realize bi-directional power flow especially due to lose the *LLC* resonant behavior due to low voltage gain under backward power transfer (Pledl *et al*. 2010). To overcome this problem, a new *LLC* resonant converter used to realize bi-directional power control and balance secondary-side currents is presented in Fig. 1(b). Comparing the circuit structures between Figs. 1(a) and 1(b), an additional switch S and inductor L_b are adopted on the primary (high voltage) side in Fig. 1(b) to allow the presented *LLC* converter to have high voltage gain and so achieve bi-directional power flow operation. Two center-tapped rectifiers with one current balance magnetic-coupling component are also adopted on the low voltage side for the high current output. The magnetic-coupling current balance element (Liu *et al*. 2016) is employed to balance currents i_{s1} and i_{s2}. If i_{s1} and i_{s2} are balanced, then the induced voltages of *CB* component are zero voltage. If i_{s1} and i_{s2} are unbalanced (such as $i_{s1} > i_{s2}$), then the one induced voltage V_1 of *CB* component tends to increase for the larger current i_{s1} to be lessened. Also, the other induced voltage V_2 of *CB* component decreases to get the lower current $i_{s2}$to rise. After $i_{s1} = i_{s2}$, one can obtain $V_1 = V_2 = 0$. When power flow is from V_H to V_L, S is open. L_m, L_r and C_r form a resonant tank and deliver power to low voltage side. Power devices Q_1 and Q_2 work as major power switches with soft switching operation, and $Q_3 \sim Q_6$ operate as the synchronous switches to decrease conduction losses on the secondary side. Frequency modulation is normally adopted to adjust the switching frequency according to different high-side voltage V_H and load current. In this case, the load-side voltage V_L is regulated at the desired value. When power flow is from V_L to V_H, the switch S is closed. L_b, L_r and C_r are operated as a *LLC* resonant tank and deliver power to primary side. Power devices $Q_3 \sim Q_6$ operate as major power switches with soft switching operation on the low voltage side, and Q_1 and Q_2 are turned off. The anti-parallel diodes D_{Q1} and D_{Q2} operate as voltage doubler rectifier synchronous switches on the high voltage side.

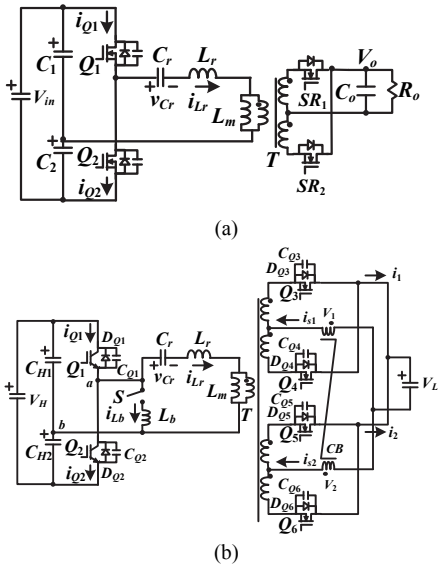

Fig. 1 The circuit configuration of resonant converter (a) conventional *LLC* converter with synchronous switches (b) the proposed *LLC* converter with bidirectional power flow and a current balance magnetic-coupling component.

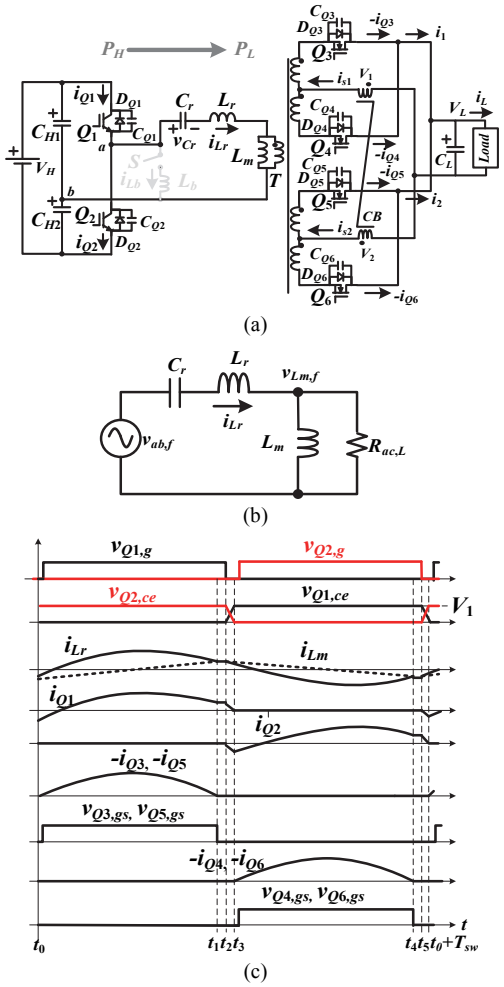

Fig. 2 The proposed converter under forward power flow operation (a) equivalent circuit (b) ac equivalent circuit by C_r, L_r, L_m and low-side ac equivalent resistance $R_{ac,L}$ (c) main pulse-width modulation waveforms under forward power flow.

2.1 Forward Power Transfer

If the power switch S is off, then power flow is from V_H to low voltage V_L, as shown in Fig. 2(a). Half bridge circuit including switches Q_1 and Q_2 on the primary side are operated by frequency-control to produce a square voltage waveform on terminal v_{ab}. For different load and input voltage conditions, the switching frequency of Q_1 and Q_2 is modulated in order to keep the load voltage constant. Synchronous switches $Q_3 \sim Q_6$ are adopted on the secondary (high current) side to decrease conduction losses. L_m, L_r and C_r are worked as series resonant tank to achieve the advantage of zero voltage operation of main switches Q_1 and Q_2. Two center-tapped rectifiers with one current balance magnetic-coupling component are employed on the high current (secondary) side to decease the current stresses on $Q_3 \sim Q_6$ and also balance two secondary-side currents i_{s1} and i_{s2}. Fig. 2(b) illustrates ac circuit of series resonant tank for forward power flow operation. Due to the fact that the input impedance of resonant tank is related to the switching frequency, the ac voltage gain $v_{Rac,L}$ / v_{ab} can be regulated by frequency control such that low voltage V_L can be controlled at the wanted voltage value. Fig. 2(c) provides the main pulse-width modulation waveforms under forward power transfer. According to the switching states of $Q_1 \sim$

Q_6, the presented converter has four (or six) operating steps for every switching period if f_{sw} > (or <) f_{r1} (series resonant frequency). The circuit operations for forward power transfer are discussed as follows. And the step circuits corresponding to six steps are shown in Fig. 3.

Step 1 [$t_0 \sim t_1$]: Before t_0, $i_{Lr} < 0$ and C_{Q1} (C_{Q2}) is discharged (charged). At t_0, $v_{CQ1} = 0$ and $i_{Lr}(t_0) < 0$. Thus, D_{Q1} conducts, and the collector-to-emitter voltage $v_{Q1,ce}$ is equal to zero. Then, switch Q_1 is turned on after t_0 so as to realize zero voltage switching. In step 1, $v_{ab} = V_H/2$, $i_{Lr} > i_{Lm}$, $v_{Lm} = nV_L$ and i_{s1} and i_{s2} are positive. Thus, D_{Q3} and D_{Q5} are forward biased. The gate voltages of synchronous switches Q_3 and Q_5 are forced to positive voltage value to reduce the conduction losses. Under the balance currents condition $i_{s1} = i_{s2}$, the induced voltages V_1 and V_2 of *CB* equal zero. If $i_{s1} > i_{s2}$, then the induced voltages V_1 of *CB* component increases to reduce i_{s1} and the V_2 decreases to rise i_{s2}. Thus, the secondary-side currents i_{s1} and i_{s2} become more balanced. Since $v_{Lm} = nV_L$ where n is turn-ratio of transformer T, i_{Lm} increases in step 1. The magnetizing current variation $\Delta i_{Lm,1}$ in step 1 is calculated as $nV_L\Delta t_{\text{step1}}/L_m$ where Δt_{step1} is time interval in step 1, and L_m is the magnetizing inductance. L_r and C_r resonant with frequency $f_{r1} = 1/2\pi\sqrt{L_r C_r}$ under $v_{ab} = V_H/2$ and $v_{Lm} = n_{VL}$. If f_{sw} > (or <) f_{r1}, the next step is going to be step 2 (or step 3).

Step 2 [$t_1 \sim t_2$]: Since $f_{sw} > f_{r1}$, the secondary-side currents i_{s1} and i_{s2} fall to zero at t_1. Thus, synchronous switches Q_3 and Q_5 are turned off. i_{Lr} flows through switch Q_1, capacitor C_r, and inductors L_r and L_m. Since $C_{H1} >> C_r$, only L_m, C_r and L_r resonant in this step with resonant frequency $f_{r2} = 1/2\pi\sqrt{(L_m + L_r)C_r}$. Switch Q_1 turns off at $t_2 = Tsw/2$.

Step 3 [$t_2 \sim t_3$]: At $t = t_2 \approx T_{sw}/2$, switch Q_1 is off. Since the primary-side current i_{Lr} at t_2 is positive and $i_{Lr}(t_2) = i_{Lm,p}$, v_{CQ1} increases and v_{CQ2} decreases. The peak magnetizing current can be calculated as:

$$i_{Lm,p} \approx nV_L/(4L_m f_{sw}) \tag{1}$$

In this step, the voltage of C_{Q2} decreases to zero, the discharged time Δt_{step3} in step 3 is calculated as:

$$\Delta t_{step3} \approx \frac{2V_H C_{Q2}}{i_{Lm,p}} = \frac{8L_m f_{sw} V_H C_{Q2}}{nV_L} \le t_d \tag{2}$$

where t_d is dead time. Under the given t_d, f_{sw}, V_H, and V_L, $L_{m,\max}$ is calculated in (3).

$$L_{m,max} \le nV_L t_d / (8 f_{sw} V_H C_{Q2}) \tag{3}$$

Step 4 [$t_3 \sim t_4$]: At t_3, the output capacitor C_{Q2} is released to zero. Since i_{Lr} at time t_3 is positive, D_{Q2} is conducting to flow the primary-side current. After time t_3, $_{Q2}$ turns on to realize soft switching operation. In step 4, $v_{ab} = -V_H/2$, $i_{Lr} < i_{Lm}$, $v_{Lm} = -nV_L$ and i_{s1} and i_{s2} are negative. Therefore, D_{Q4} and D_{Q6} conduct. The synchronous switches Q_4 and Q_6 are turned on to lessen the conduction losses. Since $vL_m = -nV_L$ in this step, i_{Lm} decreases. L_r and C_r resonant in step 4 with frequency $f_{r1} = 1/2\pi\sqrt{L_r C_r}$.

Step 5 [$t_4 \sim t_5$]: Step 5 starts at time t_4 when is1 and i_{s2} decrease to zero current and stops at time t_5 when switch Q_2 turns off. The circuit operation in step 5 likes the circuit operation is step 2. L_m, L_r and C_r resonant with frequency $f_{r2} = 1/2\pi\sqrt{(L_m + L_r)C_r}$.

Step 6 [$t_5 \sim t_0 + T_{sw}$]: The circuit operation in step 6 is similar to the circuit operation is step 3. Step 6 starts at time t_5 when Q_2 turns off and stops at time $t_0 + T_{sw}$ when C_{Q1} is discharged to zero voltage.

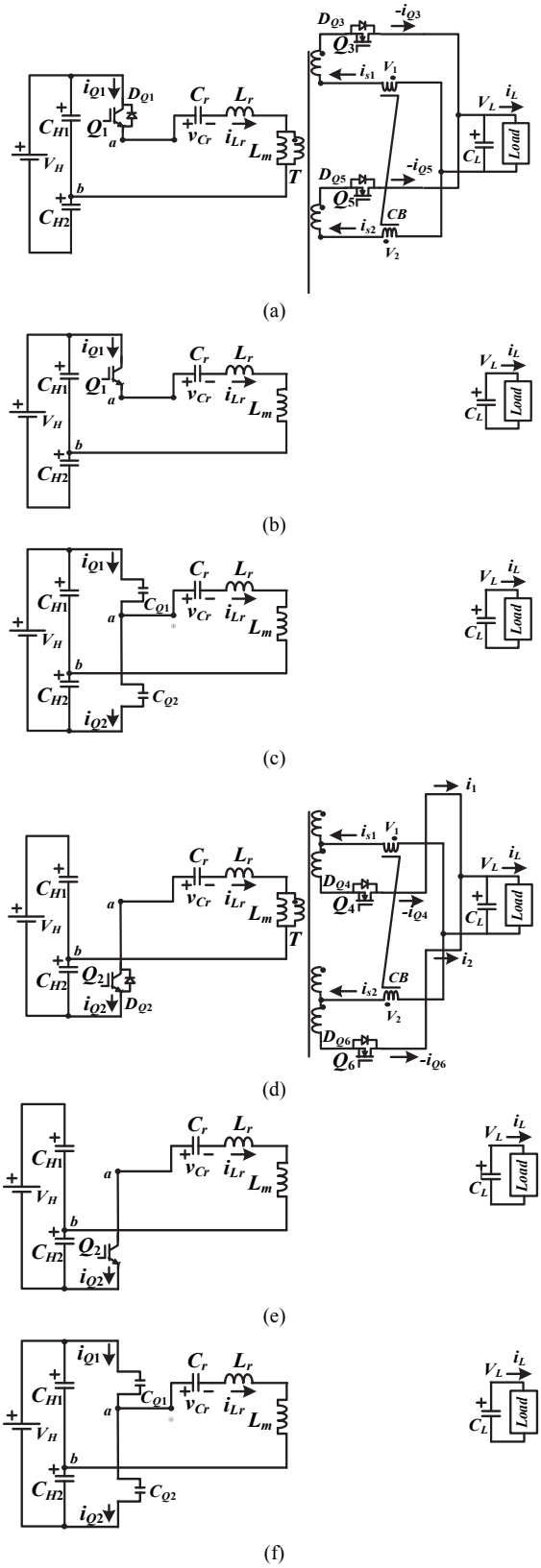

Fig. 3 Corresponding step circuits underr forward power transfer (a) step 1 (b) step 2 (c) step 3 (d) step 4 (e) step 5 (f) step 6.

The current balance magnetic-coupling component is presented to accomplish current balance. Therefore, a magnetic-coupling component is employed on the secondary (high current) side to achieve current balance. The Analysis of Fundamental Frequency (Steigerwald, 1988) is normally employed to approximate ac voltage gain versus switching frequency. Due to switching states of power switches $Q_1 \sim Q_6$, two square voltage signals are noted on the primary-side vab (with $V_H/2$ and $-V_H/2$) and v_{Lm} (with nV_L and $-nV_L$). The resonant tank, L_m, L_r and C_r, works as a filter to suppress harmonic currents. Therefore, a quasi-sinusoidal current is obtained on the resonant tank if $f_{sw} = f_{r1}$. Based on the fundamental frequency analysis, the primary-side square voltages v_{ab} and v_{Lm} can be treated as fundamental ac voltages $v_{ab,f}$ and $v_{Lm,f}$ only to make circuit analysis simpler. According to the fourier series analysis, the fundamental voltages $v_{ab,f}$ and $v_{Lm,f}$ can be obtained as $\sqrt{2}V_H/\pi$ and $2\sqrt{2}nV_L/\pi$, respectively. The load resistance $R_{o,L}$ is reflected in the primary-side of transformer to obtain ac equivalent resistor $R_{ac,L} = 8n^2R_{o,L}/\pi^2$. The ac equivalent resistance $R_{ac,L}$ is paralleled with the magnetizing inductance L_m. Figure 2(b) shows the equivalent circuit of the presented converter at forward power operation. The voltage gain is calculated as follows:

$$G_{H2L}(s) = \frac{v_{Lm,f}(s)}{v_{ab,f}(s)} = \frac{2nV_L}{V_H} = \frac{\dfrac{sL_mR_{ac,L}}{sL_m + R_{ac,L}}}{\dfrac{sL_mR_{ac,L}}{sL_m + R_{ac,L}} + \dfrac{1}{sC_r} + sL_r} \quad (4)$$

$$|G_{H2L}(f_{sw})| = \frac{K_F F^2}{\sqrt{[Q_F K_F F(F^2-1)]^2 + [(K_F+1)F^2 - 1]^2}} = \frac{2nV_L}{V_H} \quad (5)$$

where $K_F = L_m/L_r$, $F = f_{sw}/f_{r1}$, $f_{r1} = 1/(2\pi\sqrt{L_rC_r})$ and $Q_F = \sqrt{L_r/C_r}/R_{ac,L}$. The suitable switching frequency f_{sw} can be obtained from (5) under the given V_H, V_L, K_F and $R_{ac,L}$.

2.2 Backward Power Transfer

The presented converter can operate at reverse power flow with an additional inductor L_b connected at the primary side to realize the function of the *LLC* converter with zero voltage operation. Fig. 4(a) gives the circuit schematic of the presented circuit topology at reverse power operation. On the high voltage side, Q_1 and Q_2 turn off and S is on. D_{Q1} and D_{Q2} and capacitors C_{H1} and C_{H2} operate as a voltage doubler rectifier topology. Power switches $Q_3 \sim Q_6$ work as major switches to create the positive and negative voltage levels on v_{Lm}. L_b, L_r and C_r operate as a *LLC* resonant circuit to achieve soft switching operation for $Q_3 \sim Q_6$ and control V_H at the desired voltage. According to the primary-side currents i_{Lr} and iLmb, D_{Q1} and D_{Q2} are forward or reverse biased and a quasi-square waveform can be obtained on v_{ab}. Fig. 4(b) gives the ac equivalent circuit for reverse power flow. Fig. 4(c) depicts the main pulse width modulation waveforms under backward power transfer. Like the circuit operation of forward power operation, six operation steps can be observed for every switching period. Fig. 5 presents the simplified equivalent circuits for these six steps.

Step 1 [$t_0 \sim t_1$]: This step starts at t_0 when $v_{CQ3} = vC_{Q5} = 0$ and ends at t_1 when $i_{QD1} = i_{QD2} = 0$. Due to $i_{Q3}(t_0)$ and $i_{Q5}(t_0)$ are negative and $i_{Lr} > i_{Lb}$, D_{Q3}, D_{Q5} and D_{Q1} conduct. Therefore, Q_3 and Q_5 turn on after t_0 to realize zero voltage operation. In this step, $v_{ab} = v_{Lb} \approx V_H/2$, $v_{Lm} = nV_L$, i_{Lb} and i_{Lm} increase, and C_r and L_r resonant with frequency $f_{r1} = 1/2\pi\sqrt{C_rL_r}$.

Step 2 [$t_1 \sim t_2$]: Step 2 starts at time t_1 when D_{Q1} is reverse biased. i_{Lr} flows through C_r, S, L_b, T and L_r. In step 2, C_r, L_b and L_r resonant with frequency $f_{r3} = 1/2\pi\sqrt{(L_b + L_r)C_r}$.

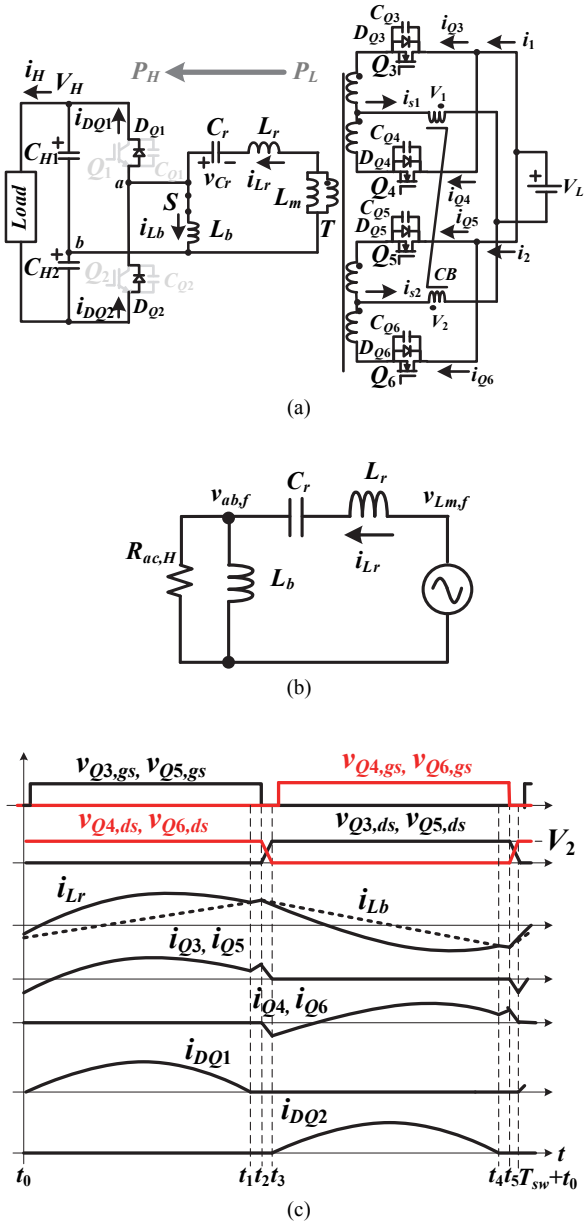

Fig. 4 The proposed circuit at reverse power flow operation (a) circuit operation (b) ac equivalent circuit of resonant tank by C_r, L_r, L_b and high-side ac equivalent resistance $R_{ac,H}$ (c) main pulse-width modulation waveforms under reverse power flow.

Step 3 [$t_2 \sim t_3$]: Step 3 starts at time t_2 when Q_3 and Q_5 are turned off. When Q_3 and Q_5 turn off, i_{s1} and i_{s2} are changed to negative value. C_{Q3} and C_{Q5} (C_{Q4} and C_{Q6}) are charged (discharged) in this step. The zero voltage switching condition of Q_4 and Q_6 is obtained as:

$$(L_b + L_r)\, i_{Lb,p}^2 + L_m i_{Lm,p}^2 > 4C_{Q,oss} V_L^2 \tag{6}$$

where $C_{Q,oss} = C_{Q3} = .. = C_{Q6}$, $i_{Lm,p} \approx nV_L/(4L_m f_{sw})$ and $i_{Lb,p} \approx V_H/(8L_b f_{sw})$. The discharged time Δt_{step3} in this step is calculated as:

$$\Delta t_{step3} \approx \frac{4V_L C_{Q,oss}}{n[i_{Lm,p} + i_{Lb,p}]} = \frac{32L_m L_b f_{sw} V_L C_{Q,oss}}{n(L_m V_H + 2nL_b V_L)} \le t_d \tag{7}$$

where td is a dead time between Q_3 and Q_4.

Step 4 [$t_3 \sim t_4$]: This step starts at t_3 when $v_{CQ4} = v_{CQ6} = 0$. In step 4, $i_{s1}(t_3)$ and $i_{s2}(t_3)$ are negative such that D_{Q4} and D_{Q6} are off. Switches Q_4 and Q_6 turn on after t_3 to achieve soft switching. Due to D_{Q2} conduct, it can be obtained that $v_{ab} = v_{Lb} \approx -V_H/2$, $v_{Lm} = -nV_L$, and L_r and C_r resonant with frequency $f_{r1} = 1/2\pi\sqrt{C_r L_r}$. Both inductor currents i_{Lm} and i_{Lb} decrease.

Step 5 [$t4 \sim t5$]: Step 5 begins at t_4 when D_{Q2} is reverse biased. In step 5, C_r, L_b and L_r resonant with frequency $f_{r2} = 1/2\pi\sqrt{(L_b + L_r)C_r}$.

Step 6 [$t_5 \sim T_{sw} + t_0$]: At time t_5, Q_4 and Q_6 turn off. i_{s1} and i_{s2} become positive value. C_{Q3} and C_{Q5} are discharged and C_{Q4} and C_{Q6} are charged in this step. The soft switching condition of Q_3 and Q_5 is similar to switches Q_4 and Q_6 in (6). At time $T_{sw} + t_0$, $v_{CQ3} = v_{CQ5} = 0$ and circuit goes to next switching period.

Based on the conducting states of $Q_3 \sim Q_6$ and D_{Q1} and D_{Q2}, it can obtain two square voltage waveforms on v_{ab} and v_{Lm}. The resonant tank, L_b, L_r and C_r, work as a filter to suppress harmonic currents. It can be calculated that the fundamental voltages $v_{Lm,f} = 2\sqrt{2}\, nN_L/\pi$ and $v_{ab,f} = \sqrt{2}\, V_H/\pi$. The ac load resistance $R_{ac,H}$ is represented as $R_{ac,H} = 2R_{o,H}/\pi^2$ and $R_{o,H}$ is load resistance on high voltage side. $R_{ac,H}$ is paralleled with L_b and the equivalent circuit at backward power flow operation is given in Fig 4(b). The voltage gain is calculated as:

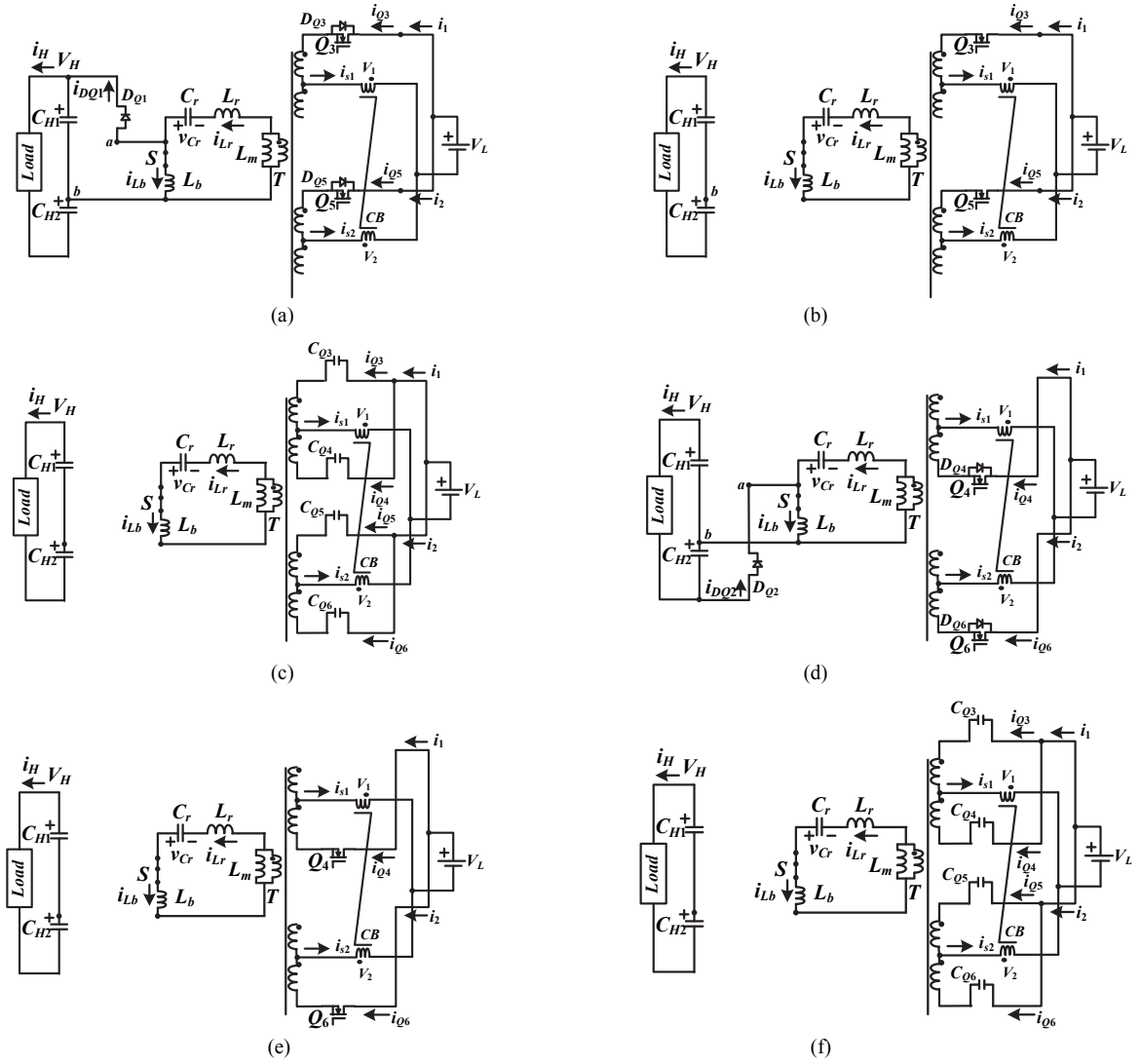

Fig. 5 Corresponding step circuits underr reverse power flow operation (a) step 1 (b) step 2 (c) step 3 (d) step 4 (e) step 5 (f) step 6.

$$G_{L2H}(s)| = \frac{v_{ab,f}(s)}{v_{Lm,f}(s)} = \frac{V_H}{2nV_L} = \frac{\dfrac{sL_bR_{ac,H}}{sL_b+R_{ac,H}}}{\dfrac{sL_bR_{ac,H}}{sL_b+R_{ac,H}}+\dfrac{1}{sC_r}+sL_r} \quad (8)$$

$$|G_{L2H}(f_{sw})| = \frac{K_BF^2}{\sqrt{[Q_BK_BF(F^2-1)]^2+[(K_B+1)F^2-1]^2}} = \frac{V_H}{2nV_L} \quad (9)$$

where $K_B = L_b/L_r$, $F = f_{sw}/f_{r,1}$, $Q_B = \sqrt{L_r/C_r}/R_{ac,H}$ and $f_{r,1}=1/(2\pi\sqrt{L_rC_r})$.

3. DESIGN PROCEDURES

The design example is presented and discussed in this section. Bi-directional power flow can be achieved in the proposed circuit. Under forward power flow, input voltage V_H is between 350 V and 400 V and output voltage V_L = 48 V. The rated load current is 15 A. Under backward power flow, the input voltage V_L = 44 V to 52 V and V_H = 400 V with 720 W rated power. The series resonant frequency is selected as 100 kHz. The voltage transfer functions of forward and backward power flow in (5) and (9) are similar. Therefore, it can only consider the forward or backward power flow operation to derive the circuit parameters. In the following, the main circuit parameters are calculated under forward power operation. The voltage gain $|G_{H2L}|$ at V_H = 400 V and V_L = 52 V conditions is fixed at unity. From (5), the turn-ratio n is expressed in (10).

$$n = \frac{V_H}{2V_L} = \frac{400}{2\times 52} \approx 3.85 \quad (10)$$

Transformer T is implemented with 23 primary winding turns and 6 secondary winding turns with EER 42 ferrite core. Due to the actual selected winding turns, the maximum and minimum dc gains at the input voltage range and 48 V output voltage are expressed as:

$$|G_{H2L}|_{\max} = \frac{2nV_{L,nom}}{V_{H,\min}} \approx 1.05 \quad (11)$$

$$|G_{H2L}|_{\min} = \frac{2nV_{L,nom}}{V_{H,\max}} \approx 0.92 \quad (12)$$

In (5), the inductor ratio K_F and quality factor Q_F should be tradeoff to have low circulating current loss and high voltage gain. In this example, K_F = 10 and Q_F = 0.6 are selected to have a peak gain higher than 1.05 and to control low-side voltage stable at 48 V. The ac equivalent resistance $R_{ac,H}$ is calculated at the rated power.

$$R_{ac,L} = \frac{8n^2}{\pi^2}R_{o,L} \approx 38.11\ \Omega \quad (13)$$

According the desired series resonant frequency f_{r1} = 100 kHz, the L_r and C_r are calculated as $L_r = QR_{ac,L}/(2\pi f_r) \approx 36.4\mu H$ and $C_r = 1/(4\pi^2L_rf_r^2) \approx 70nF$. The magnetizing inductance $L_m = K_F \times L_r$ = 364 H. The voltage ratings of Q_1 and Q_2 equal $V_{H,\max}$ = 400 V and the voltage ratings of $Q_3 \sim Q_6$ equal two times of maximum output voltage $2V_{L,\max}$ = 104 V. The IRG4PC40W with 600 V rating / 20 A rating are used for Q_1 and Q_2, and IRFB4321PbF with 150 V rating / 85 A rating are used for $Q_3 \sim Q_6$. Two SiHG20N50C with 500 V rating / 20 A rating are used to achieve ac switch S. The parallel inductor Lb is selected as 216 μH to have inductor ratio $K_B = L_b/L_r$ = 6 under reverse power flow operation. The input capacitances C_{H1} and C_{H2} are 330 μF/400 V and C_L = 4400 μF/100 V. The main idea of the current balance magnetic-coupling is based on the concept that the primary and secondary winding current ratio is related to the turn-ratio of transformer under the steady-state. The unity turn-ratio is used on the prototype. Therefore, the primary and secondary currents are identical if the magnetizing inductance is larger enough. The current balance current-coupling transformer is built with EER 42 ferrite core and 46 turns on both of the primary and secondary sides with 1mH magnetizing inductance. The ac switch S is implemented with two power MOSFETs G20N50C by back to back connection. The control block of the proposed converter in the prototype circuit is demonstrated in Fig. 6. First, the high side and low side voltages, V_H and V_L, are measured and compared with the reference voltages, $V_{H,ref}$ and $V_{L,ref}$. The power flow selection can decide the power low from V_H to V_L or from V_L to V_H. The voltage controller based on a voltage control oscillator can generate the gating signals with variable frequency based on the voltage error between the sensed voltage and reference voltage. PWM generator produces the necessary gating signals $Q_1 \sim Q_6$ and S according to the power flow selection signal and the gating signal from voltage control oscillator.

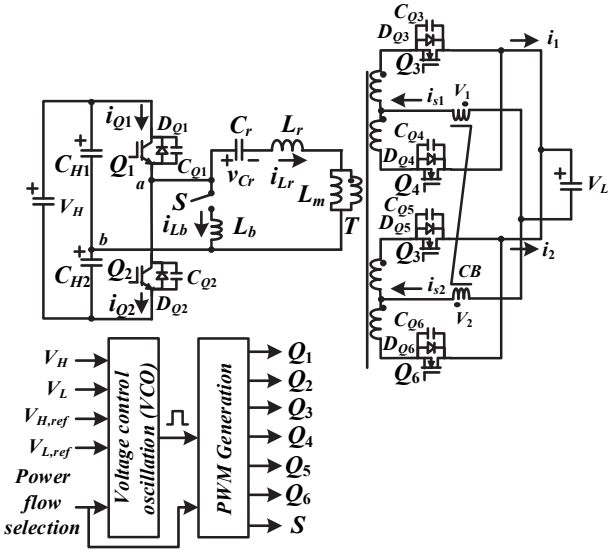

Fig. 6 The control block of the proposed converter in the prototype circuit.

4. EXPERIMENTAL RESULTS

According to the developed prototype circuit, the validated test results are presented in previous section. Figs. 7 ~ 13 demonstrate the experimental results for forward power operation. Fig. 7 gives the measured waveforms of devices Q_1 and Q_2 and input split voltages V_{CH1} and V_{CH2} under 350 V and 400 V input and rated power condition. Clearly, it is observed that the switching frequency at V_H = 400 V is greater than V_H = 350 V. Fig. 8 shows the experimental results of v_{ab}, v_{Cr} and i_{Lr} under different input voltages and rated power. Figs. 9 and 10 illustrate the measured waveforms of the main switches Q_1 and Q_2 at light (20%) load. For both switches, they are turned on at zero voltage switching from light (20%) load. Likewise, the experimental results of $-i_{Q3}$ ~ $-i_{Q6}$ at the rated load current are presented in Fig. 11. Q_3 ~ Q_6 are all turned off under zero current. The output currents of two center-tapped rectifiers at full load are shown in Fig. 12. Due to the fact that the current balance magnetic-coupling component is used on the secondary-side, two output currents i_1 and i_2 are balanced well for different input voltage cases. Fig. 13 demonstrates the measured results of split voltages and low side voltage at rated power. The input split capacitor voltages are balanced well. Figs. 14 ~ 18 provide the measured results under reverse power operation. The results obtained frommain switches Q_3 and Q_3 and resonant voltage and current at the rated power and different low-side voltages are demonstrated in Fig. 14. The switching frequency at 52 V input is higher than 44 V input so as to both obtain lower voltage gain of the resonant converter and maintain high-side voltage at 400 V. Fig. 15 provides the experimental waveforms of $-i_{Lr}$, i_{Lb}, i_{DQ1} and i_{DQ2} at the rated power. When $i_{Lr} > i_{Lb}$, diode D_{Q1} conducts. On the other hand, D_{Q2} conducts if $i_{Lr} > i_{Lb}$. If $i_{Lr} = i_{Lb}$, both diodes D_{Q1} and D_{Q2} are reverse biased. Figs. 16 and 17 demonstrate the experimental waveforms of the main switches Q_3 and Q_4 at 20% load. It is clear to see that both switches are turned on at soft switching from 20% load. However, the turn-off of hard switching is observed on Q_3 and Q_4 due to high switch current when Q_3 and Q_4 are turned off. Power switches Q_5 and Q_6 have same turn-on and turn-off characteristics as Q_3 and Q_4 at reverse power flow operation. Fig. 18 shows the measured results of low side voltage and split capacitor voltages at rated power and reverse power flow condition. The split capacitor voltages are balanced well. Figs. 19 and 20 show the measured switching frequency and circuit efficiencies of the studied converter under different loads. The measured switching frequencies at forward power flow operation are 78 kHz, 72.5 kHz and 65 kHz under V_H = 350 V input case and 144 W, 360 W and 720 W, respectively. For V_H = 400 V input, the measured switching frequencies are 128 kHz, 109 kHz and 98 kHz at 144 W, 360 W and 720 W, respectively. The measured circuit efficiencies are 94.9% at 144 W, 93.9% at 360 W and 93.2% at 720 W. The test switching frequencies at reverse power flow operation are 79 kHz at 144 W, 71 kHz at 360 W and 66 kHz at 720 W under V_L = 44 V input. For V_L = 52 V input, the test switching frequencies are 121 kHz at 144 W, 105 kHz at 360 W and 92 kHz at 720 W. The test efficiencies are 91.2% at 144 W, 90.5% at360 W and 89.6% at 720 W.

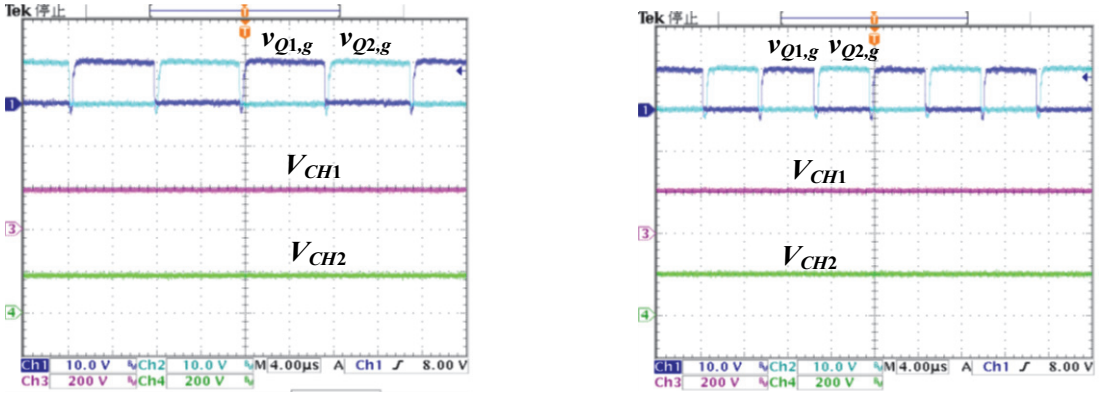

Fig. 7 Measured results of main switches and input split voltages at forward power flow under the rated power (a) V_H = 350 V (b) V_H = 400 V.

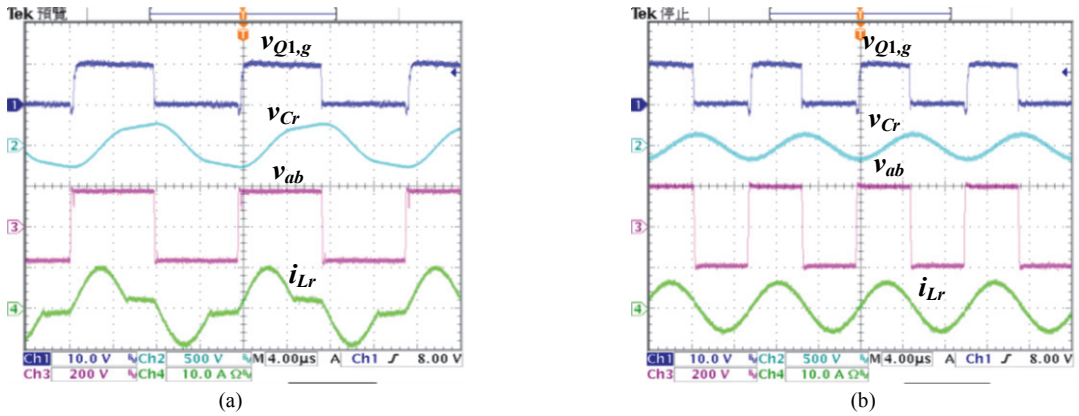

Fig. 8 Measured results of the ac side voltage and resonant voltage and current of the *LLC* resonant tank under the rated power (a) V_H = 350 V (b) V_H = 400 V.

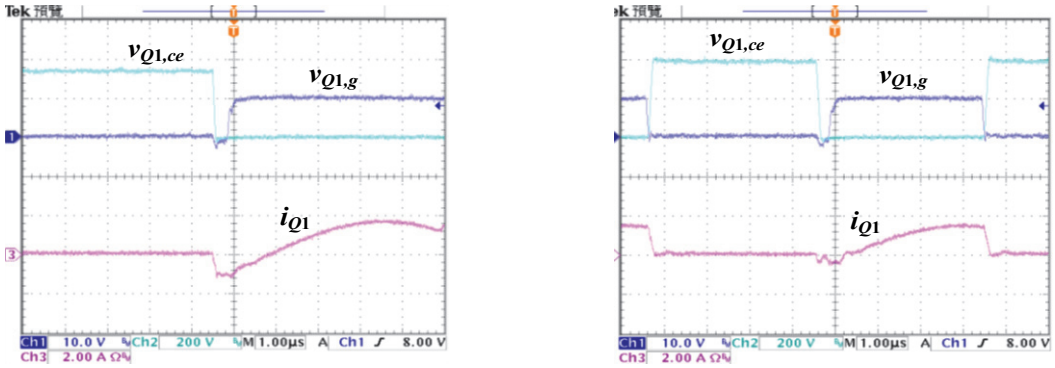

(a) (b)

Fig. 9 Measured results of switch Q_1 at 20% load (a) V_H = 350 V (b) V_H = 400 V.

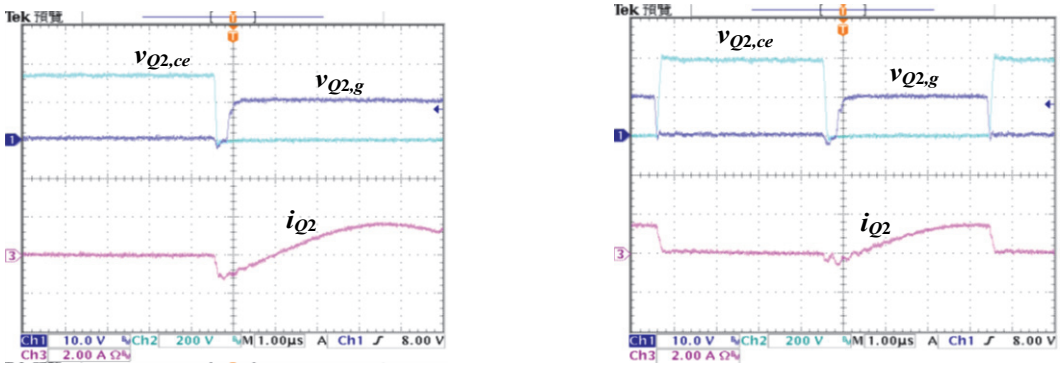

(a) (b)

Fig. 10 Measured results of switch Q_2 at 20% load (a) V_H = 350 V (b) V_H = 400 V.

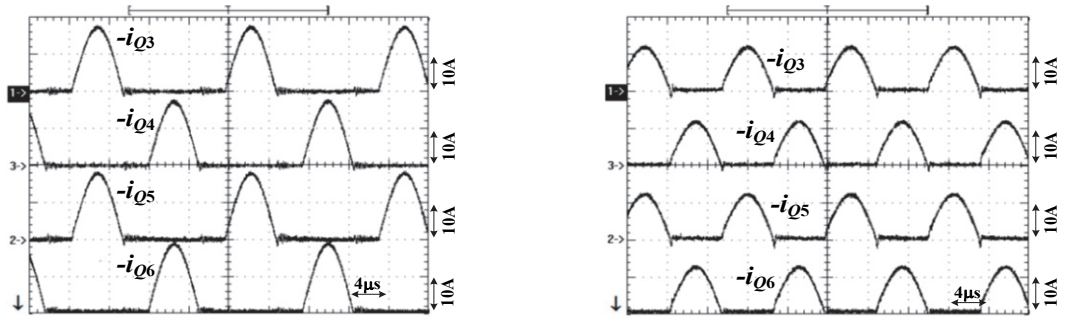

(a) (b)

Fig. 11 Measured results of the low voltage side currents rent of the *LLC* resonant tank under the rated power (a) V_H = 350 V (b) V_H = 400 V.

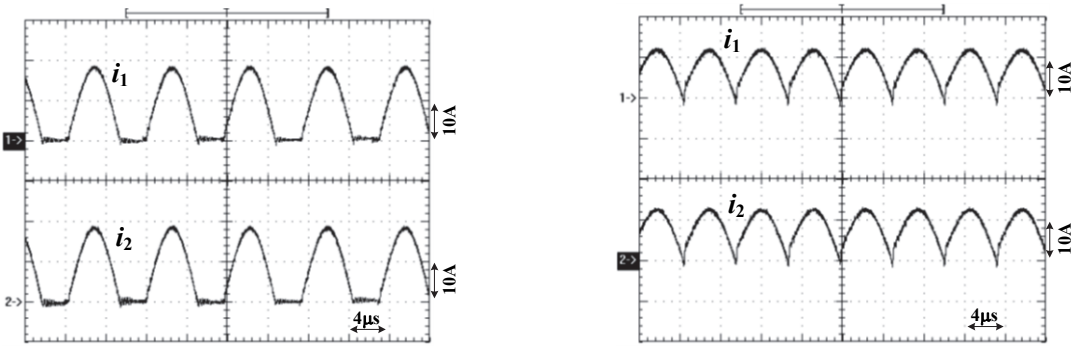

(a) (b)

Fig. 12 Measured results of the output currents of two center-tapped rectifiers at the rated power (a) V_H = 350 V (b) V_H = 400 V.

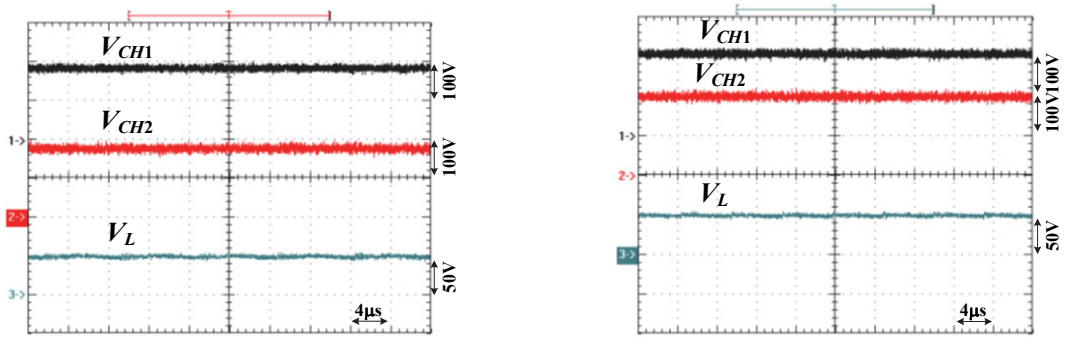

Fig. 13 Measured results of split voltages and low side voltage at rated power (a) V_H = 350 V (b) V_H = 400 V.

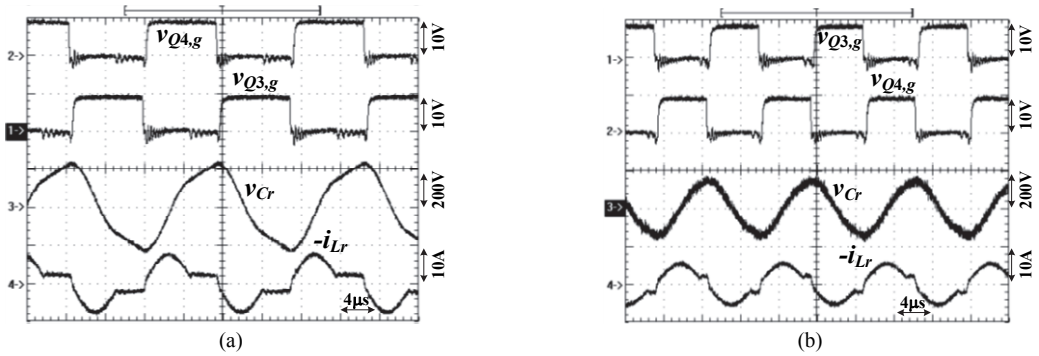

Fig. 14 Measured results of the main switches Q_3 and Q_4 and resonant voltage and current at reverse power flow operation and the rated power (a) V_L = 44 V (b) V_L = 52 V.

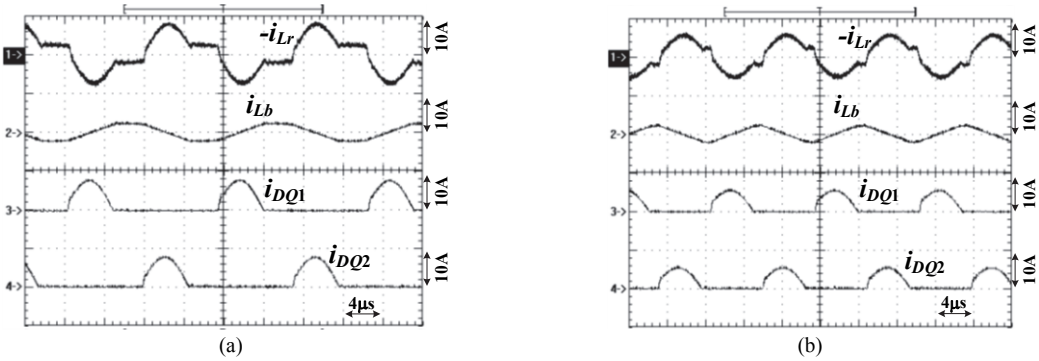

Fig. 15 Measured results of the resonant current, inductor current and diode currents at reverse power flow operation and the rated power (a) V_L = 44 V (b) V_L = 52 V.

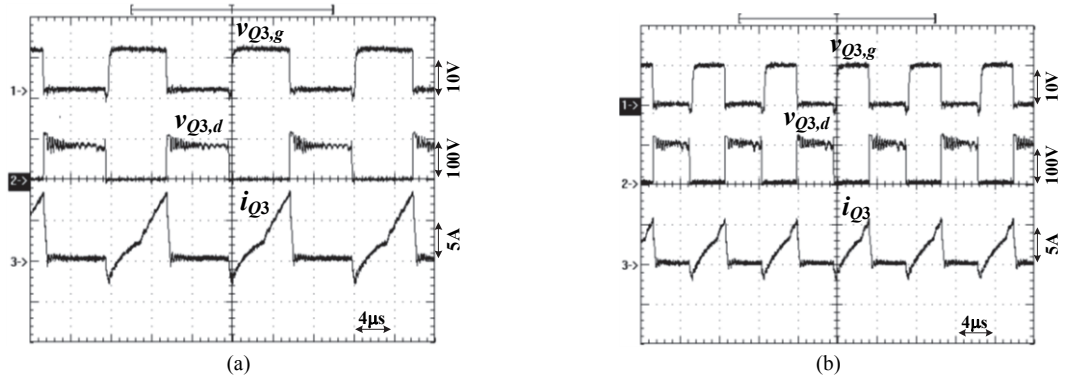

Fig. 16Measured results of switch Q_3 at 20% load (a) V_L = 44 V (b) V_L = 52 V.

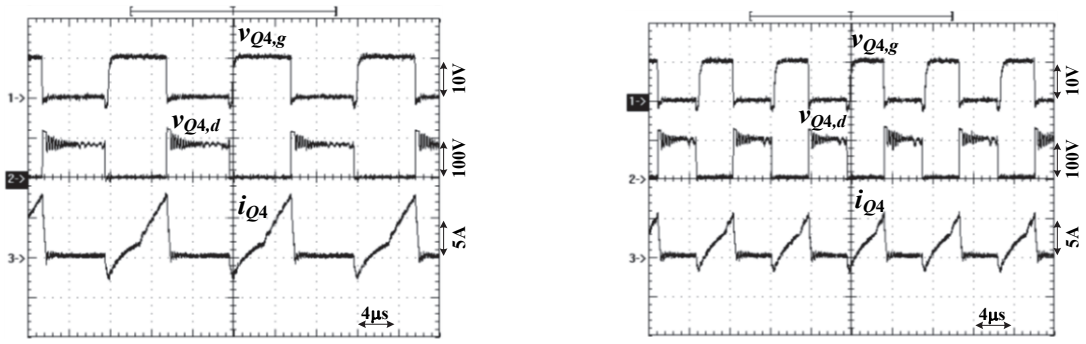

Fig. 17 Measured results of switch Q_4 at 20% load (a) V_L = 44 V (b) V_L = 52 V.

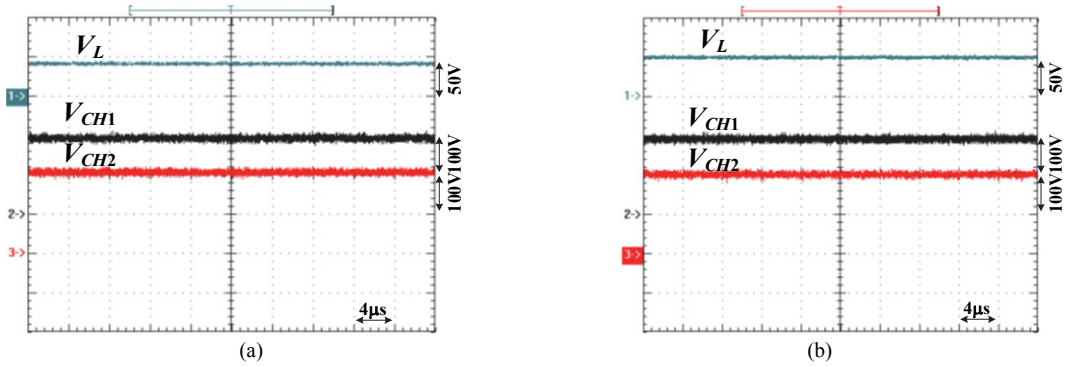

Fig. 18 Measured results of low side voltage and split voltages at rated power (a) V_H = 350 V (b) V_H = 400 V.

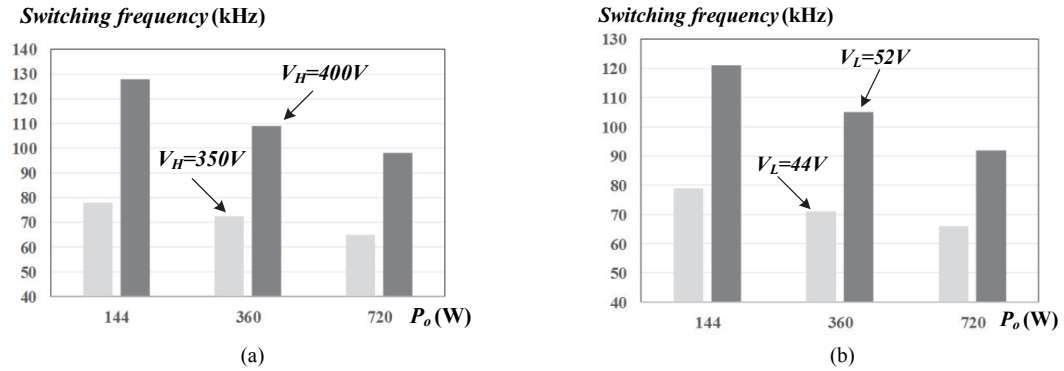

Fig. 19 Measured switching frequencies under (a) forward power flow (b) reverse power flow.

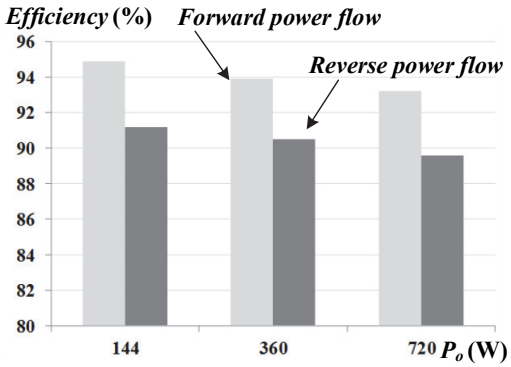

Fig. 20 Measured switching frequencies under different operation conditions.

5. CONCLUSIONS

A dc-dc LLC soft switching converter between high voltage 400 V and low voltage 48 V was determined to accomplish zero voltage operation and achieve bidirectional power transfer. The prototype circuit had one half bridge leg on the primary side and two full-wave rectifiers on the secondary (high current) side. A current balance magnetic-coupling core was employed on the high current side to achieve current sharing. To realize the LLC resonant behavior for the power flows of both directions, the additional switch and inductor were used on the primary side. Frequency-control was adopted to adjust the switching frequency in order to keep load voltage at the desired voltage. At forward power operation, the additional inductor was disconnected to the primary side to eliminate the unnecessary circulating current on primary side. Under the reverse power operation, an additional inductor was connected on the input half bridge leg to accomplish the LLC resonant behavior and soft switching operation. Finally, the obtained experimental results verify, the achievability of the studied soft switching converter.

REFERENCES

Ahrabi, R.R., Ardi, H., Elmi, M., and Ajami, A. (2017). "A novel step-up multi input dc-dc converter for hybrid electric vehicles application." *IEEE Trans. Power Electron*., **32**(5), 3549-3561.

Emadi, A., Lee, Y.J., and Rajashekara, K. (2008). "Power electronics and motor drives in electric, hybrid electric, and plug-in hybrid electric vehicles." *IEEE Trans. Ind. Electron*., **55**(6), 2237-2245.

Jiang, T., Zhang, J., Wu, X., Sheng, K., and Wang, Y. (2015). "A bidirectional LLC resonant Converter with automatic forward and backward mode transition." *IEEE Trans. Power Electron*., **30**(2), 757-770.

Kim, E.S., Park, J.H., Jeon, Y.S., Kong, Y.S., Lee, S.M., and Kim, K. (2014). "Bidirectional secondary LLC resonant converter using auxiliary switches and inductor." *In Proceedings of the APEC Conference*, 1941-1947.

Lee, J.Y., Jeong, Y.S., and Han, B.M. (2012). "A two-stage isolated/bidirectional DC/DC converter with current ripple reduction technique." *IEEE Trans. Ind. Electron*., **59**(1), 644-646.

Liu, C., Xu, X., He, D., Liu, H., Tian, X., Guo, Y., Cai, G., Ma, C., and Mu, G. (2016). "Magnetic-coupling current-balancing cells based input-parallel output-parallel LLC resonant converter modules for high-frequency isolation of dc distribution systems." *IEEE Trans. Power Electron*., **31**(10), 6968-6979.

Mangu, B., Akshatha, S., Suryanarayana, D., and Fernandes, B.G. (2016). "Grid-connected PV-wind-battery-based multi-input transformer-couple bidirectional dc-dc converter for household applications." *IEEE J. Emerg. Sel. Top. Power Electron*., **4**(3), 1086-1095.

Mishimay, T., Hiraki, E., and Nakaoka, M. (2010). "A high frequency-link bidirectional DC-DC converter for super capacitor-based automotive auxiliary electric power systems." *J. Power Electron*., **10**(1), 27-33.

Pledl, G., Tauer, M., and Buecherl, D. (2010). "Theory of operation, design procedure and simulation of a bidirectional LLC resonant converter for vehicular applications." *In Proceedings of VPPC Conference*, 1-5.

Shen, C.L., Shen, Y.S., Chiu, P.C., and Liang, T.C. (2017). "Isolated bidirectional converter with minimum active switches for high-voltage ratio achievement and micro-grid applications." *IET Proc. Power Electron*., **10**(15), 2208-2216.

Steigerwald, R. (1988). "A comparison of half-bridge resonant converter topologies." *IEEE Trans. Power Electron*., **3**(2), 174-182.

Tan, K., Yu, R., Guo, S., and Huang, A.Q. (2014). "Optimal design methodology of bidirectional LLC resonant DC/DC converter for solid state transformer application." *In Proceedings the IECON Conference*, 1657-1664.

Wu, H., Chen, L., and Yan, X. (2015). "Secondary side phase shift controlled dual transformer based asymmetrical dual-bridge converter with wide voltage gain." *IEEE Trans. Power Electron*., **30**(10), 5381-5392.

Xu, G., Sha, D., Xu, Y., and Liao, X. (2018). "Hybrid-bridge-based DAB converter with voltage match control for wide voltage conversion gain application." *IEEE Trans. Power Electron*., **33**(2), 1378-1388.

Yilmaz, M. and Krein, P.T. (2013). "Review of battery charger topologies, charging power levels, and infrastructure for plug-in electric and hybrid vehicles." *IEEE Trans. Power Electron*., **28**(5), 2151-2169.

Zhang, C., Li, P., Kan, Z., Chai, X., and Guo, X. (2018). "Integrated half-bridge CLLC bidirectional converter for energy storage systems." *IEEE Trans. Ind. Electron*., **65**(5), 3879-3889.

Zhang, Y., Gao, Y., Li, J., and Sumner, M. (2018). "Interleaved switched-capacitor bidirectional dc-dc converter with wide voltage-gain range for energy storage systems." *IEEE Trans. Power Electron*., **33**(5), 3852-3869.

Zhao, S., Li, Q., Lee, F.C., and Li, B. (2018). "High-frequency transformer design for modular power conversion from medium-voltage ac to 400Vdc". *IEEE Trans. Power Electron*., **33**(9), 7545-7557.

Zou, S., Lu, J., Mallik, A., and Khaligh, A. (2018). "Bi-directional CLLC converter with synchronous rectification for plug-in electric vehicles." *IEEE Trans. Ind. Applic*., **54**(2), 998-1005.